Hindawi
Advances in Civil Engineering
Volume 2021, Article ID 9927922, 17 pages
https://doi.org/10.1155/2021/9927922

Research Article

Experimental Study on Lateral Bearing Mechanical Characteristics and Damage Numerical Simulation of Micropile

Ning Liu,[1,2] **Yi-Xiong Huang**,[2] **Bo Wu**,[1] **and Wei Huang**[1]

[1]*College of Civil Engineering and Architecture, Guangxi University, Nanning 530004, China*
[2]*College of Civil Engineering, Guizhou University, Guiyang 550025, China*

Correspondence should be addressed to Ning Liu; nliu1@gzu.edu.cn

Received 19 March 2021; Revised 26 June 2021; Accepted 22 July 2021; Published 26 August 2021

Academic Editor: Zetian Zhang

The construction site of the foundation pit support project in the urban area is narrow. Micropile has the advantages of flexible pile position layout, strong site adaptability, and fast construction speed, which can effectively control the horizontal displacement of the foundation pit and ensure the safety of surrounding buildings. However, the lateral bearing capacity of micropile is weak. In order to study the lateral force characteristics and failure characteristics of micropile, laboratory tests on the flexural and tensile strength of reinforced concrete micropiles with different diameters and with or without external steel pipes were performed. The authors studied the lateral force characteristics and failure characteristics of various types of micropiles. Based on numerical simulation software ABAQUS, the measured yield strength of the specimen was used as the loading force. And taking the occurrence and development of concrete damage into consideration, the loading process was simulated. The result shows the following: (1) the micropile specimens with external steel pipe had better flexural performance than the bare micropiles and the mechanical characteristics of the specimens changed from brittleness to plasticity; (2) the degree of concrete damage is greatly reduced after the external steel pipe is attached, and the bearing capacity of the micropile specimen of the same diameter is increased by 70% after the external steel pipe is added; and (3) the specimens were mainly damaged due to tensile damage. The calculation formula for the lateral bearing capacity of the concrete-filled steel tube micropile considering the damage is proposed through fitting analysis. The calculation formula, the finite element calculation value, and the calculation formula proposed by other scholars are compared with the authors' test and the test data of other scholars. The meta-calculation results, experimental results, and formula calculation results proposed by the authors have high accuracy.

1. Introduction

Micropile generally refers to small-diameter bored piles with a pile diameter of 70~300 mm, which have large slenderness ratio. Usually, micropiles are formed by drilling, installing steel pipes or steel cages, grouting, and other construction technologies. The construction speed is fast and has certain antisliding effect. Only light construction machines and tools are needed during construction, which have the advantages of flexible pile placement, fast construction speed, strong adaptability to construction sites, and little impact on the environment. However, due to the complex engineering geological conditions of the rock mass, the horizontal bearing capacity of micropiles with small cross-section size is weak, which greatly limits the development of this technology [1].

Scholars have conducted research on the seismic performance of micropile reinforcement and the reinforcement mechanism of different geological conditions [2–10]. In addition, other scholars have also conducted circular and square micropile concrete flexural, tensile, and resistance research work on torsion performance and have achieved certain scientific results [11–16]. Foundation pit support engineering is often restricted by the surrounding environment. The foundation pit is close to existing buildings (structures), and the construction disturbance of large equipment will cause the foundation deformation of the buildings along the street and affect the safety of the building. In a small site, there is no space for grading, and it does not meet the construction conditions of large equipment. Therefore, in this case, the optimal plan is to use

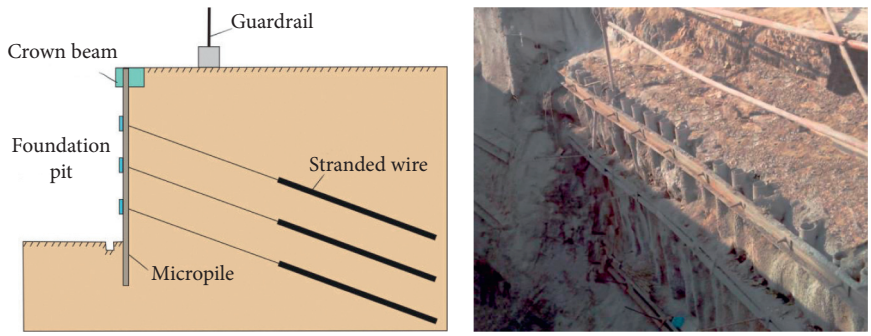

Figure 1: Micropile combined supporting structure and its engineering application. (a) Structure of micropile combined supporting. (b) Micropile supporting foundation pit.

microsteel pipe piles for combined support, as shown in Figures 1(a) and 1(b). In response to the problems encountered in the construction of backfilling unconsolidated soil and loose soil in deep foundation pit projects with narrow construction sites, Dong and Zhang [17] proposed a combined supporting structure of frame prestressed anchor microsteel piles. The laboratory similar model test of a single row of micropile was carried out by Wang [18] who studied and analyzed the failure characteristics of the micropile soil system and the corresponding laws of the micropile mechanics. The laboratory similar model test of the influence of lateral load on the micropile group was carried out by Hussain et al. [19]. The effects of pile length-to-diameter ratio, sand relative density, and pile group spacing on the lateral bearing capacity of micropiles were studied. Furthermore, the mechanical behavior of pile groups subjected to lateral load was evaluated. Li et al. [20] placed micropiles on cement piles, moderately weathered rock formations, and strongly weathered rock formations and conducted onsite monitoring. It was found that the bending moments of the micropile in the three types of formations all appeared in the middle and lower parts of the pile, showing a "bulging-belly" curve. The micropile can bear a large bending moment in the cement pile, which can effectively reduce the horizontal displacement of the foundation pit. However, it mainly plays a role of presupport in moderately weathered rock formations and strongly weathered rock formations. Kershaw and Luna [21] conducted comparative experiments on micropiles subjected to horizontal loads in loose and dense sand, respectively. It is found that the influence of sand density on the load deflection behavior of laterally loaded piles is much greater than the lateral stiffness (casing thickness) of micropiles. The performance changes of the micropiles installed in loose sand seem to be independent of the lateral structural stiffness of the micropiles. The reason may be that the lower stiffness of the sand controls the behavior of the pile, so the main response of the pile is rotation, not bending. Liu and Li [22] conducted numerical simulations to study the applicability of micropile in rock foundation pits. It has been found that the micropile bears greater bending moment and axial force in thicker strongly weathered rock formations or inferior rock formations, so it can effectively reduce the horizontal displacement of the foundation pit. He et al. [23] proposed a simplified calculation model for the micropile based on the force relationship between the micropile steel pipe, the anchor solid, and the soil. The actual foundation pit support project is calculated as an example, and the treatment method is given. The theoretical calculations are verified by onsite monitoring of foundation pit support.

It can be seen from the above research that the micropile mainly exerts its lateral bearing capacity when supporting the foundation pit. However, the flexural resistance of micropile is weak. The focus of this study is how much lateral bearing capacity the micropile can provide in foundation pit support engineering, as well as the deformation and failure characteristics of its lateral load. The flexural and tensile mechanical properties of reinforced concrete micropile with external steel tube and bare-reinforced concrete micropile were compared and analyzed through laboratory model tests. In addition, in order to further study its lateral bearing capacity, the relationship between the lateral bearing capacity of the micropile and the cross-sectional size, external steel pipe, and concrete damage and failure is explored.

2. Experimental Study

2.1. Test Overview. In this experiment, 18 specimens were designed, including 9 reinforced concrete short column specimens(LGH) with nominal dimensions of $3 \times d \times L = 3 \times 140 \times 1500$ (mm), $3 \times d \times L = 3 \times 168 \times 1500$ (mm), $3 \times d \times L = 3 \times 203 \times 1500$ (mm) and 9 concrete-filled steel tube short column specimens(GGH) with nominal dimensions of $3 \times d \times t \times L = 3 \times 140 \times 4.5 \times 1500$ (mm), $3 \times d \times t \times L = 3 \times 168 \times 4.5 \times 1500$ (mm), and $3 \times d \times t \times L = 3 \times 203 \times 4.5 \times 1500$ (mm), where d is the cross-sectional diameter, t is the wall thickness of the steel tube, and L is the length of the specimen. The test steel pipe is made of Q235 steel, and the but weld is designed according to GB/50017-2017 [24].The fabrication of concrete-filled steel tube and reinforced concrete specimens are shown in Figures 2 and 3.

In order to observe the deformation and failure of the specimens conveniently, a 50 mm × 50 mm grid was drawn on the outer surface of the processed reinforced concrete micropile and concrete-filled steel tube micropile specimens.

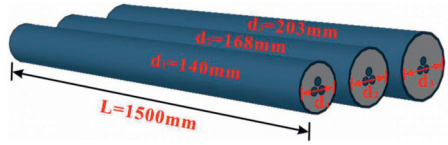

Figure 2: Model diagram of the test micropile specimen.

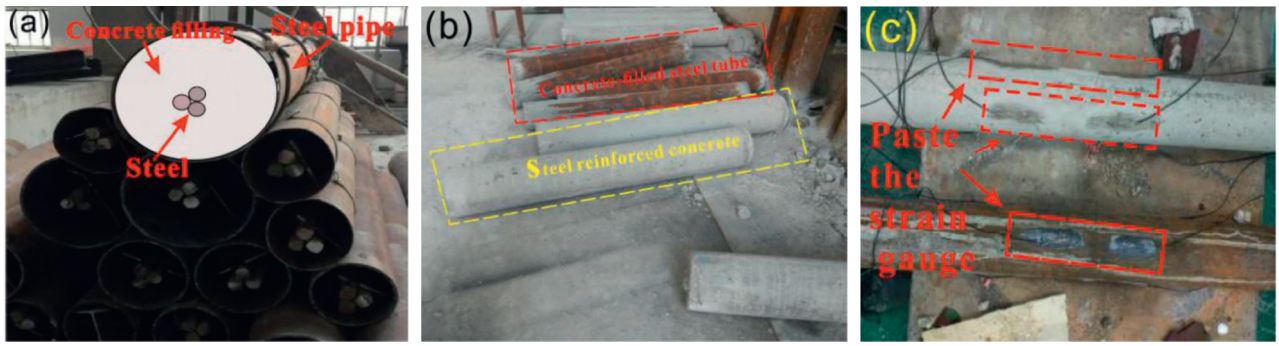

Figure 3: Fabrication of the test loading specimen. (a) Making of test pieces. (b) LGH and GGH of the specimen. (c) Pasting the strain gauge.

The external steel pipes and built-in steel bars of the micropile are shown in Figure 3(a). Before pouring concrete, the cover plate at one end of the steel pipe was welded, then the steel pipe was erected, concrete was poured from the top of the test piece, the concrete was vibrated and compacted; finally, the concrete surface was leveled with the section of the steel pipe. The prepared test piece is shown in Figure 3(b). Concrete standard cube test pieces and prism test pieces were made at the same time, and the test pieces were naturally cured and watered regularly. After curing the concrete for 28 days, the concrete surface was ground flat with a grinding machine.

C30 commercial concrete was adopted. The mix proportion composition of the concrete is shown in Table 1.

2.2. Test Methods. Before the test, the material properties of steel and the mechanical properties of concrete cube blocks were tested according to standard test methods. The steel plate was made into three standard specimens, and tensile tests were carried out on a tensile tester based on the method specified in GB/T228-2016 [25]. The measured yield strength of steel was $f_s = 311$ MPa, ultimate strength $f_u = 460$ MPa, elastic modulus $E_s = 2.07 \times 105$ MPa, and Poisson's ratio $v = 0.293$. The strength of C30 concrete cube test block was measured by 150 mm cube block cured under the same conditions according to GB/T50081-2016 [26], and the measured concrete cube compressive strength was $f_{cu} = 35.5$ MPa. The details of steel and concrete properties are shown in Table 2.

Various types of micropiles were tested on a YAS-2000 microcomputer-controlled electro-hydraulic servo pressure testing machine in the geotechnical laboratory of the College of Civil Engineering of Guizhou University. First, a grid is drawn on the surface of the micropile and then the reinforced concrete pile is polished with sandpaper to smooth the place where the strain gauge needs to be installed (shown in Figure 3(c) for details). Three rows of strain gauges were installed along the longitudinal direction of each pile, three pieces in each row, and then connected the strain gauge with the computer. The micropile specimen is transversely placed on a servo pressure testing machine (as shown in Figure 4), and dial gauges were installed at both ends of the specimen to measure the bending deformation displacement of the micropile. The two bearings in the middle of the servo pressure testing machine were jacked up after turning on the servo pressure testing machine, shear force was applied to the test piece, and then the loading was increased gradually until the micropile was completely destroyed. In this process, according to the test specification, the bending displacement was measured with a dial gauge, and the surface strain was measured with a strain gauge. The data on the dial gauge were recorded every 30 s. Through analyzing the test data, the ultimate bending and tensile bearing capacity of micropile were determined.

2.3. Test Phenomenon. During the test, three loading tests were carried out on the specimens with the same diameter. There are mainly two types of mechanical deformation and failure of the specimens: micropile-reinforced concrete with steel pipes attached outside and exposed micropile-reinforced concrete (without steel pipes attached outside). At that initial stage of test loading, both kinds of specimens showed good mechanical deformation. However, the difference in deformation between the two types of specimens after loading to a certain value was highlighted: the exposed micropile-reinforced concrete started to crack from 10 kN and expanded rapidly. After continuous loading, the surface crack of the specimen developed into a gap of 2-3 cm, Φ25 types of steel bars were peeled off from the concrete and then the specimen has been destroyed. The reinforced concrete with micropile attached with steel pipes showed obvious plasticity. The specimens were not damaged until the end of

Table 1: Mix design of concrete.

Concrete strength (MPa)	Cement (kg/m^3)	Sand (kg/m^3)	Water (kg/m^3)	Aggregate (kg/m^3)
C30	429	536	185	1250

Table 2: Properties of steel and concrete.

Material	$f_y(f_c)$ (MPa)	$f_u(f_{cu})$ (MPa)	$E_s(E_c)$ (MPa)	$v_s\,(v_c)$
Steel plate	311	460	2.07×10^5	0.293
C30	25.7	35.5	3.12×10^4	0.23

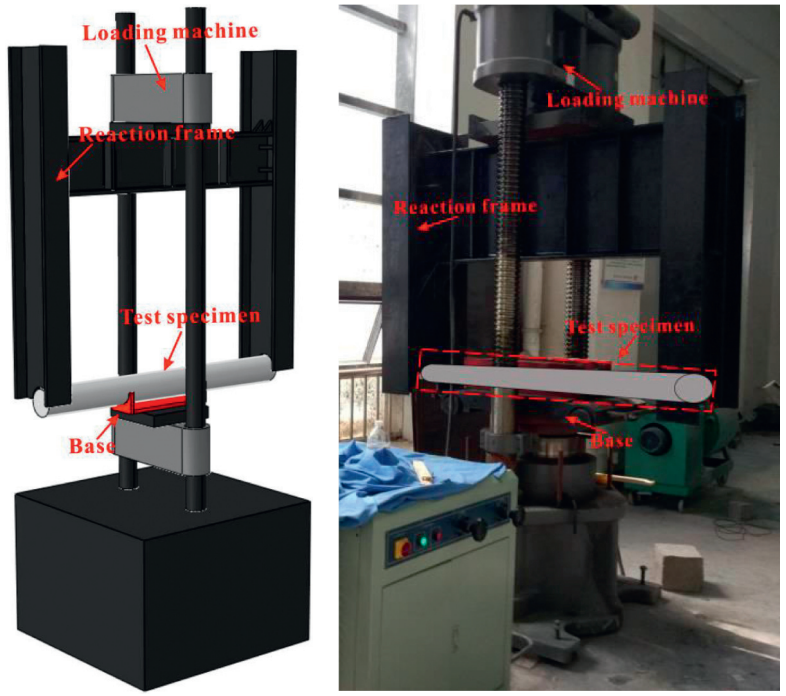

(a) (b)

Figure 4: Test equipment and loading device. (a) Loading device model. (b) Loading equipment.

loading, but the deformation was obvious. The test results of the two types of specimens are shown in Figure 5.

2.4. Analysis of Test Results. As seen from Figures 6(a)–6(c), the concrete micropile specimens without the addition of steel tube (LGH) externally show obvious brittle deformation in the bearing capacity test. At that initial stage of test loading, the micropile specimens with three diameters all show elastic deformation, but the strength of the concrete micropile specimens decreases obviously after reaching the material stresses limit as the loading continues. It shows a fluctuating decline with the increase of the displacement of the specimens. The test stops after the failure occurs. At this time, each specimen has a certain residual strength, which is related to the steel bars reserved in the concrete.

As shown in Figures 6(d)–6(f), compared with the micropile specimen without external steel pipe, the relationship between the stress and the deformation of concrete-filled steel tube micropile specimen (GGH) is the mechanical characteristic curve of plastic material: With the test loading, the specimen first presents elastic deformation, then the stress-enhancement curve changes after reaching the material yield strength. Meanwhile, the stress and deformation of the specimen are no longer linear correlation, but it mainly shows that the same loading force increase in this stage, but the deformation of the specimen is larger and more obvious than that in the initial loading stage. Therefore, the addition of concrete micropiles with steel pipes not only enhances the bearing capacity but also appears certain warning before damage, which will be safer in practical engineering.

In order to compare the bearing capacity of reinforced concrete and concrete-filled steel tube micropiles, the bearing capacity reduction factor, GL, of them has been introduced. The ratio of the ultimate bearing capacity N_{GGH} of the concrete-filled steel tube micropile to the ultimate bearing capacity N_{LGH} of the reinforced concrete micropile is

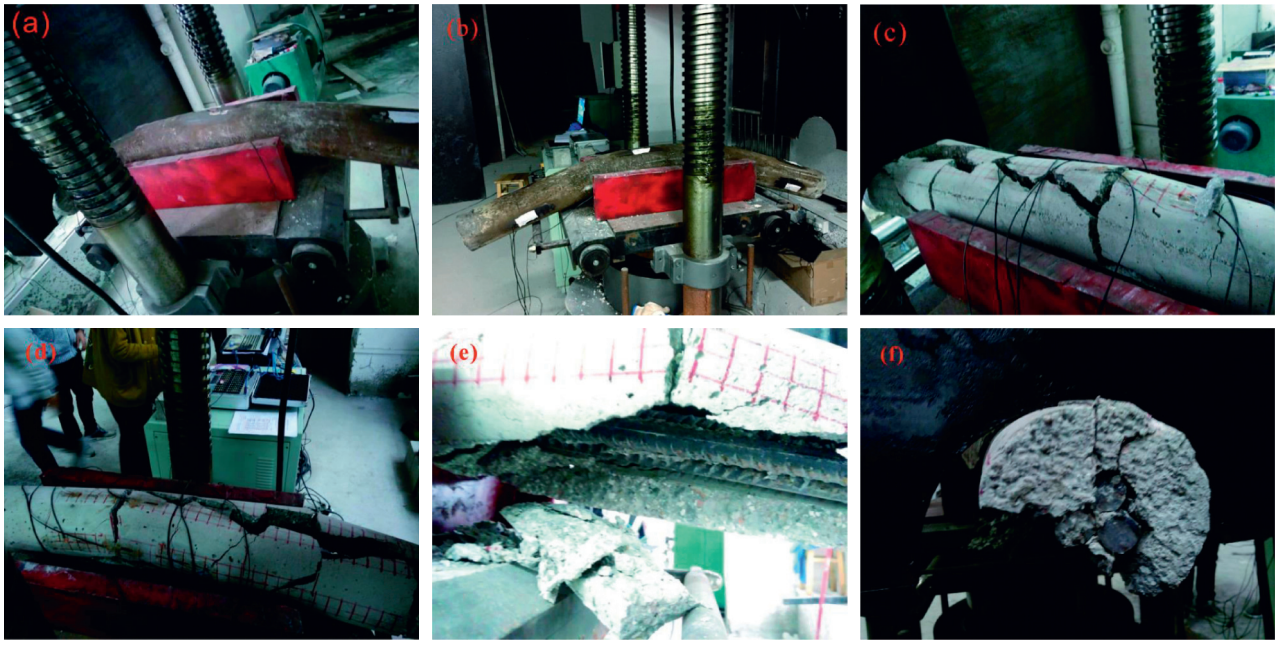

Figure 5: Deformation and failure of micropile specimens under loading. (a, b) Deformation of the specimens (GGH). (c–f) Destruction of the specimens (LGH).

$$\mathrm{GL} = \frac{N_{\mathrm{GGH}}}{N_{\mathrm{LGH}}}. \tag{1}$$

The test bearing capacity ratio LLD of exposed-reinforced concrete micropile specimens with different diameters has been introduced, and its expression is shown as follows:

$$\mathrm{LLD} = \frac{N_{\mathrm{LGH}-n_1}}{N_{\mathrm{LGH}-n_2}}. \tag{2}$$

The test bearing capacity ratio GGD of different diameter specimens of externally attached concrete-filled steel tube micropiles has been introduced, and its expression is shown as follows:

$$\mathrm{GGD} = \frac{N_{\mathrm{GGH}-n_1}}{N_{\mathrm{GGH}-n_2}}. \tag{3}$$

Figure 7 shows the test bearing capacity ratio (GL) of the reinforced concrete micropile specimen and the concrete-filled steel tube micropile specimen under the same diameter.

As can be seen from Figure 7, compared with the ultimate bearing capacity of reinforced concrete, the ultimate bearing capacity of reinforced concrete with steel pipes is obviously improved, among which the micropile with a diameter of 140 mm is increased to more than 5 times of the original ultimate strength. The micropile with a diameter of 168 mm is increased to more than 9 times of the original ultimate strength. The micropile with a diameter of 203 mm is increased to more than 15 times of the original ultimate strength. From this, it can be obtained that with the increase of diameter, the ultimate bearing capacity of concrete attached with steel pipes is more significantly enhanced. Besides, the ratio GL shows an increasing change phenomenon with the increase of the displacement of the micropile: at the initial stage of the test (the deformation of the specimen ≤20 mm), although the GL value shows an upward trend, it fluctuates obviously, which is related to the plasticity and brittleness of the specimen (after the steel tube is attached, the stress of the concrete changes from brittle deformation to plastic deformation). When the deformation is close to 20 mm, the concrete micropile with steel tube attached achieves yield, and the stress and displacement of the specimen will no longer show an approximate linear elastic relationship, so the stress change rate of the specimen will slow down. Also, the GL value will decrease. The concrete micropile with steel tube attached to it enters the stress-enhancement stage with loading the specimen continuously, so the GL value changes to increase, thus the GL value shows the phenomenon of fluctuation and increases during the overall test process.

Figure 8 shows that the test bearing capacity ratio of bare-reinforced concrete micropile specimen with different diameters. As can be seen from Figure 8, in the initial loading stage (specimen displacement <20 mm), the bearing capacity of reinforced concrete with larger diameter is higher than that of smaller reinforced concrete, which is at least 3 times higher. However, due to the change of brittleness of concrete, the specimen shows brittle failure after the loading beyond its elastic range. Therefore, the change of LLD value in Figure 8 shows a phenomenon that it decreases and then tends to be stable with the increase of displacement (LLD value eventually tends to 1). It can be seen from this that although the diameter of antislide pile is increased, the failure forms of reinforced concrete with different diameters are still very similar when its stress exceeds the bearing

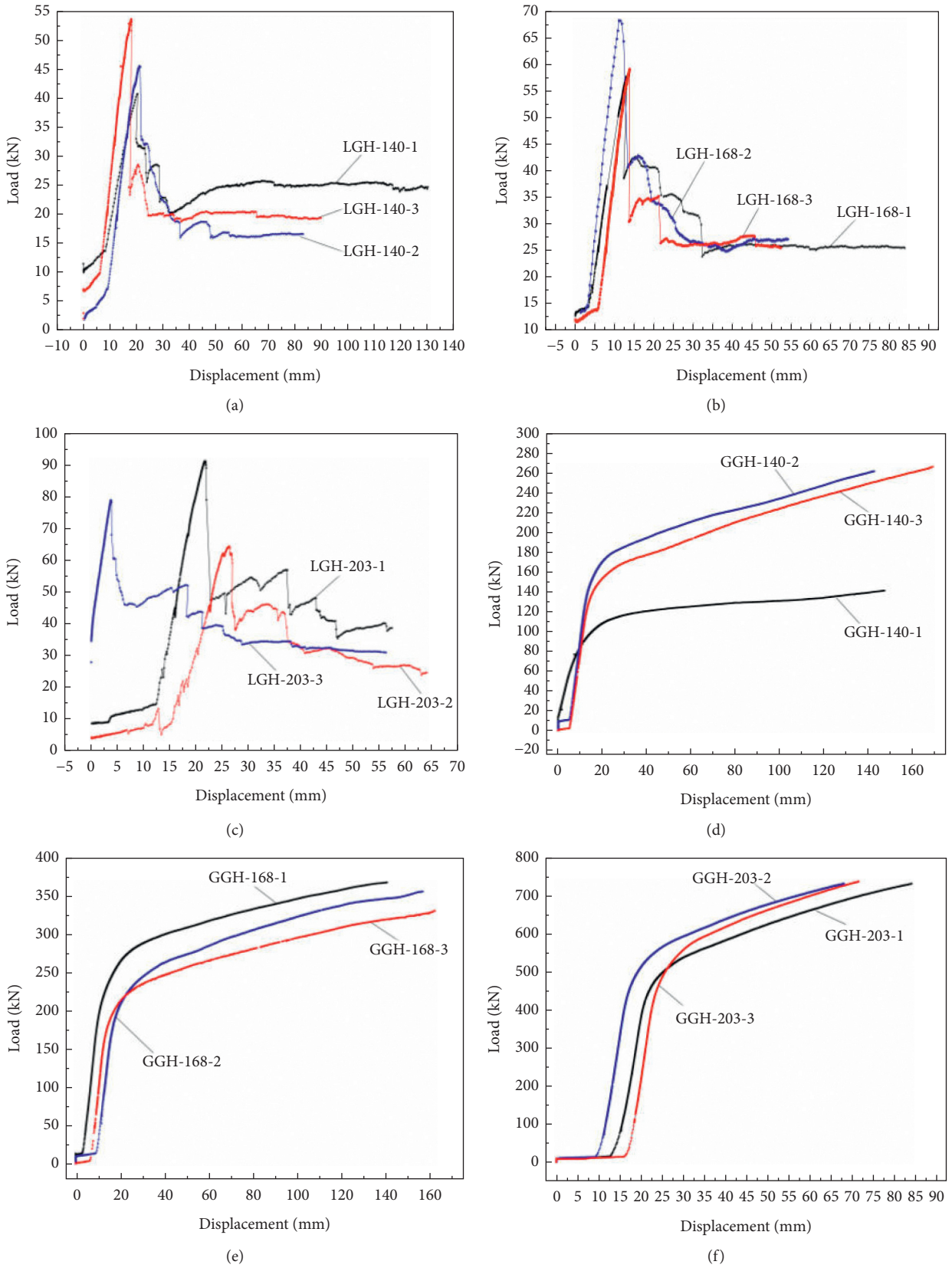

Figure 6: Loading force-displacement test results of each specimen. (a) LGH-140. (b) LGH-168. (c) LGH-203. (d) GGH-140. (e) GGH-168. (f) GGH-203.

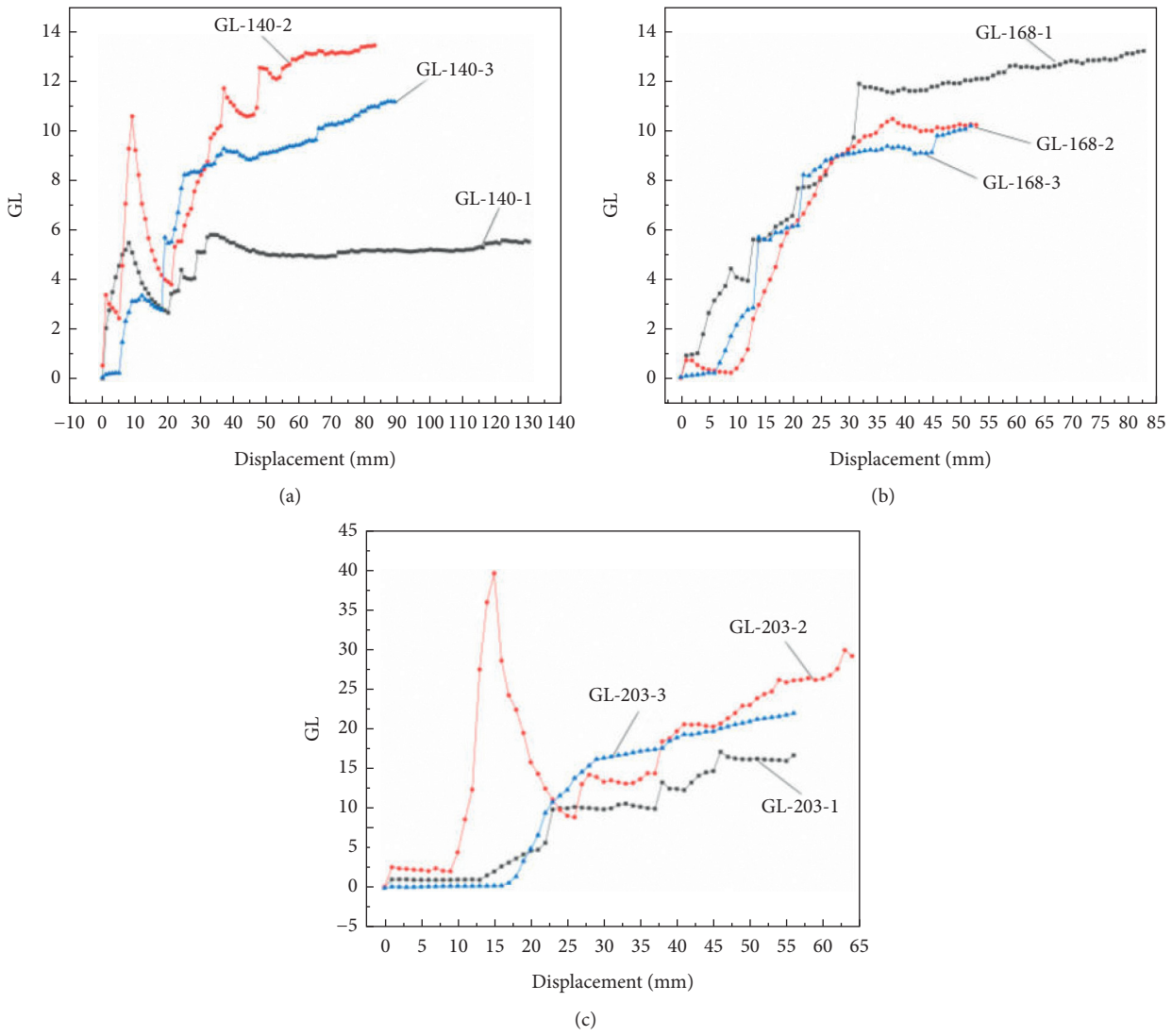

Figure 7: GL value of each specimen. (a) GL-140. (b) GL-168. (c) GL-203.

capacity in the elastic stage. Moreover, it is particularly important to add the attached steel pipes and change the mechanical stress characteristics of concrete micro antislide piles so as to transform them into plastic deformation, which is conducive to providing more obvious warning for the damage of antislide piles in physical engineering and plays a very good early warning role for the occurrence of engineering accidents.

Figure 9 shows the bearing capacity ratio of specimen with different diameters of externally attached steel tube-reinforced concrete micropile. As can be seen from Figure 9, the influence of different diameters on the bearing capacity of the micropile concrete with steel tube attached is obvious. The results show that the GGD value of the specimens with larger diameter difference is higher than that of the specimens with smaller diameter difference. The GGD value of the specimens with larger diameter difference is higher than that of the specimens with smaller diameter difference after the curve tends to be stable. Among them, the GGD values of 203 mm and 140 mm specimens reached above 3 m, which shows that increasing the diameter of antislide pile appropriately can play a greater role in bearing capacity in practical engineering. The GGD values of Figure 10 show that the elasticity increases at the initial stage of the test and increases slowly with the increase of the displacement of the specimen and then gradually tends to be stable. It shows a typical stress change curve of plastic materials, which illustrates the mechanical characteristics of micropile concrete added with externally attached steel pipes.

3. Numerical Simulation

3.1. Parameter Selection. In order to study the bearing capacity of reinforced concrete and concrete-filled steel tube, the finite element numerical software ABAQUS is selected to simulate the test process. At the same time, in order to study the working effectiveness of concrete in micropile specimens under transverse compression, the occurrence and development of damage in micropile concrete specimens are considered in the model.

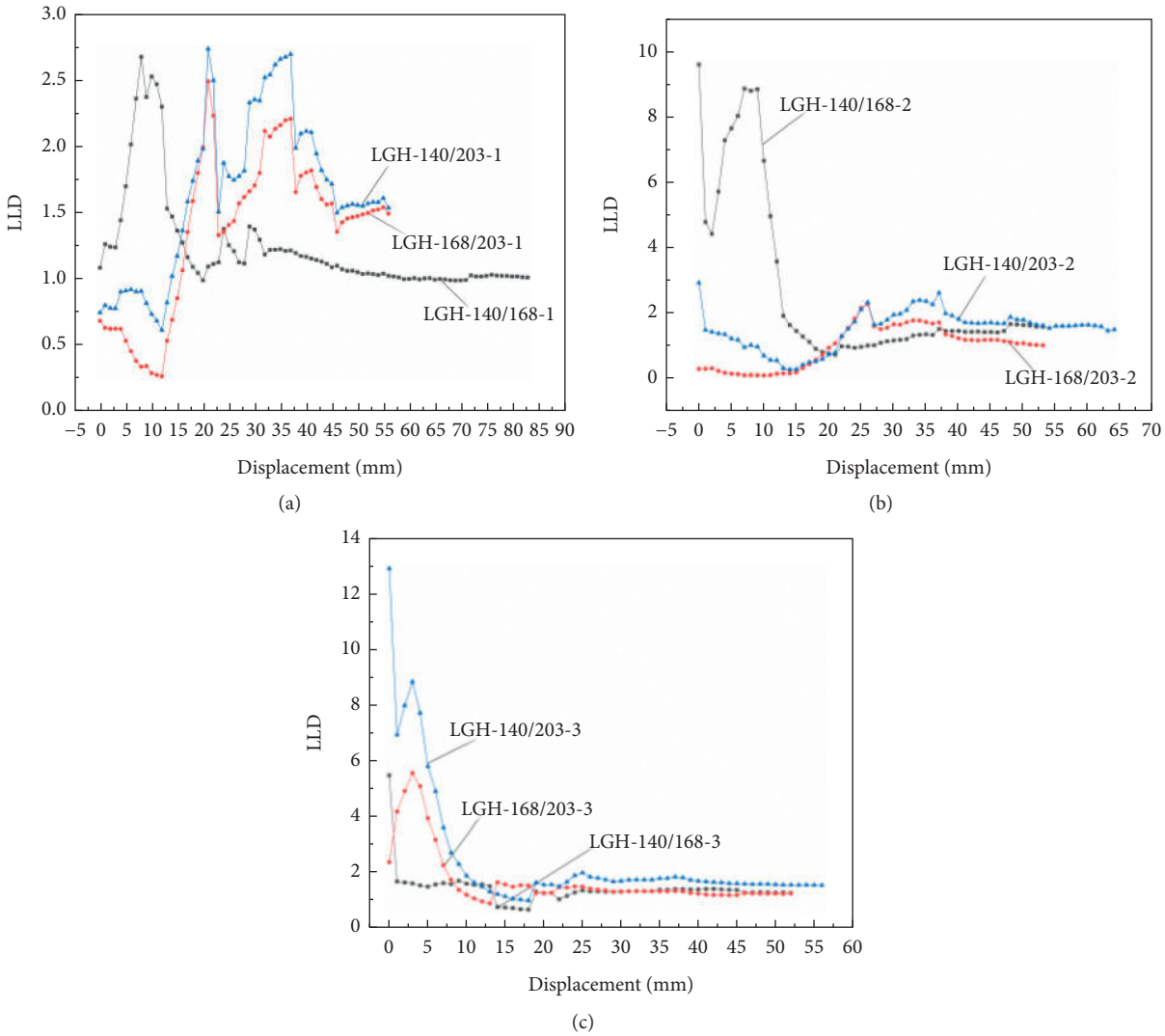

Figure 8: LLD value of each specimen. (a) LLD-1. (b) LLD-2. (c) LLD-3.

Both steel pipes and concrete are considered to be three-dimensional solid elements (C3D8R), and steel bars are adopted truss elements, which are built into concrete, as shown in Figure 10. In the model, the interface between steel tube and concrete is Coulomb friction contact. The tangent direction is penalty function. The friction coefficient is 0.8, and the normal direction is hard contact simulation. The interaction is surface-to-surface contact, and the slip mode is finite slip.

The constitutive relation of steel and concrete, including the corresponding parameter values, is shown in [27], and the specific expression is

$$y = \begin{cases} \dfrac{A_1 x + (B_1 - 1)x^2}{1 + (A_1 - 2)x + B_1 x^2}, & x \le 1, \\ \dfrac{x}{\alpha_1 (x-1)^2 + x}, & x > 1, \end{cases} \tag{4}$$

where $y = \sigma/f_c$, $x = \varepsilon/\varepsilon_c$; σ is the stress, unit MPa; f_c is the axial compressive strength, $f_c = 0.4 f_{cu}^{7/6}$; f_{cu} is the concrete cube compressive strength; ε is the strain; ε_c is the strain corresponding to peak compressive stress; $\varepsilon_c = 383 f_{cu}^{7/18} \times 10^{-6}$; A_1 and B_1 are the ascending parameters, $A_1 = 9.1 f_{cu}^{-(4/9)}$, $B_1 = 1.6(A_1 - 1)^2$; and α_1 is the descending parameter, $\alpha_1 = 0.15$.

The stress-strain relationship of steel pipe is taken as [27]

$$\sigma_i = \begin{cases} E_s \varepsilon_i, & \varepsilon_i \le \varepsilon_y, \\ f_s, & \varepsilon_y < \varepsilon_i \le \varepsilon_{st}, \\ f_s + \zeta E_s (\varepsilon_i - \varepsilon_{st}), & \varepsilon_{st} < \varepsilon_i \le \varepsilon_u, \\ f_u, & \varepsilon_i > \varepsilon_u, \end{cases} \tag{5}$$

where σ_i is the equivalent stress; $f_u = 1.5 f_s$, where f_s is the yield strength; $E_s = 2.06 \times 10^5$ MPa; ε_i is the equivalent strain; ε_y is the corresponding strain when the steel yields; ε_{st} is the corresponding strain when the steel strengthens; and ε_u is the corresponding strain when the steel reaches the ultimate strength, taking $\varepsilon_{st} = 12\varepsilon_y$, $\varepsilon_u = 120\varepsilon_y$, and $\zeta = 1/216$.

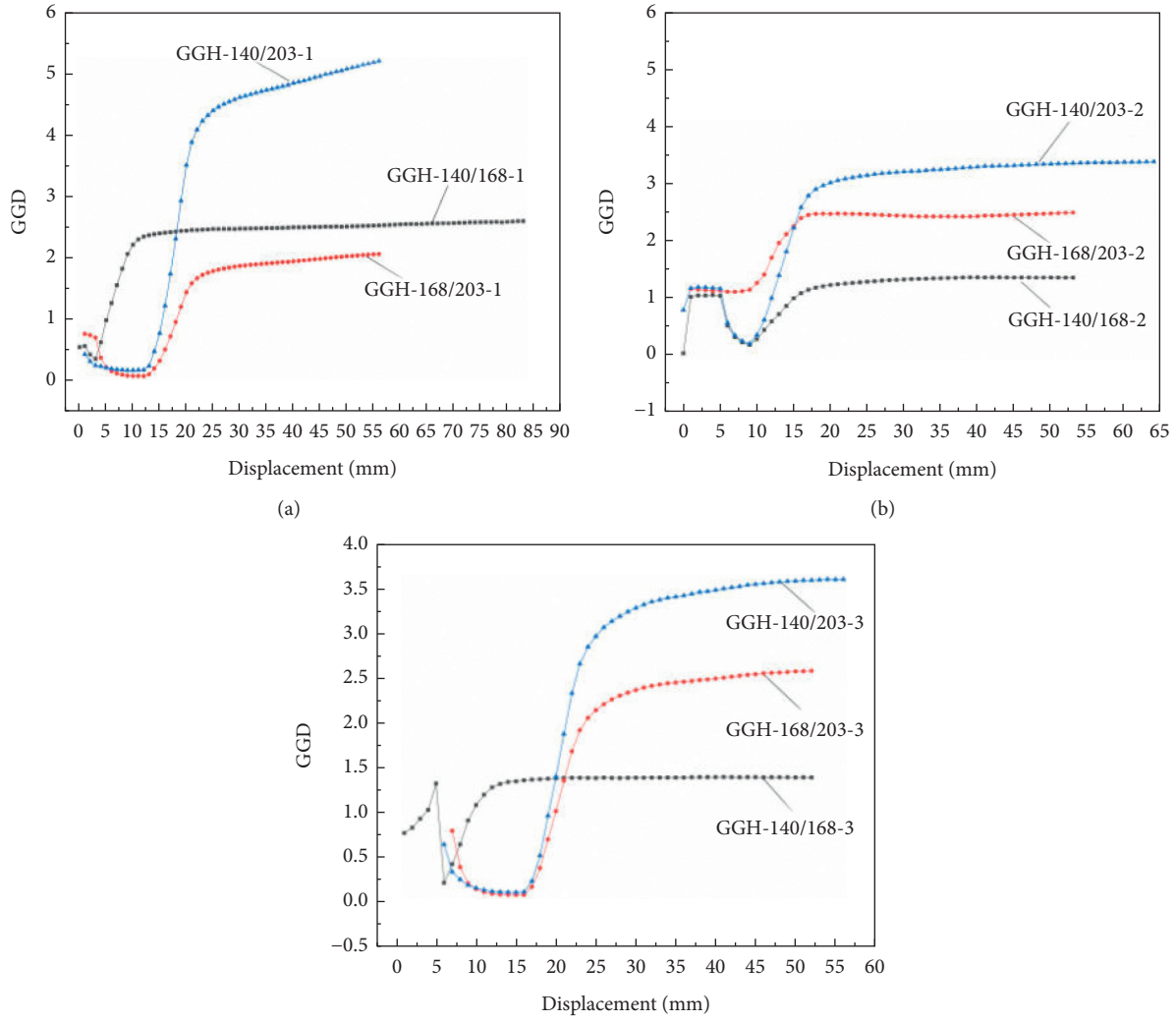

Figure 9: GGD value of each specimen. (a) GGD-1. (b) GGD-2. (c) GGD-3.

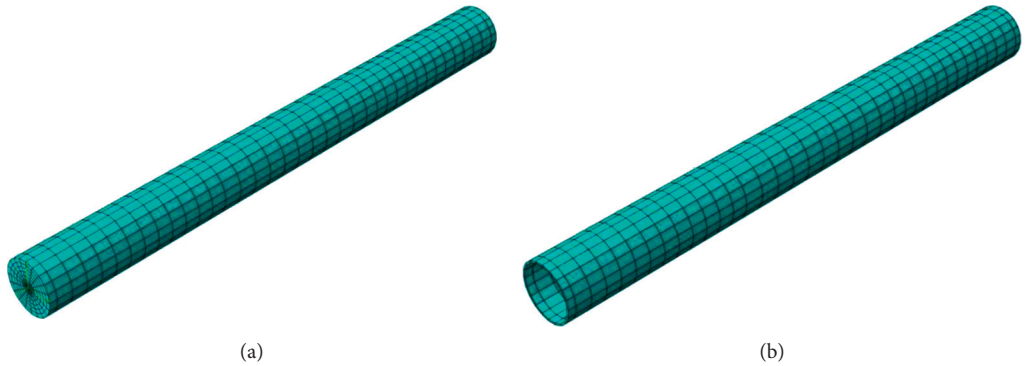

Figure 10: Model grid diagram. (a) Concrete. (b) Steel pipe.

3.2. Result Extraction and Analysis. The numerical simulation results of tensile damage of reinforced concrete of micropile without attached steel pipe are shown in Figure 11(a). As can be seen from Figure 11(a), tensile damage mainly occurs in the upper part of the specimen. After the specimen is loaded, the extension area of the upper surface of the specimen from both ends to the middle has lost its working effectiveness (the damage value in the red

area is 0.9), and the damage value gradually decreases from the upper part of the specimen to the lower part.

Figure 11(c) shows the result of numerical simulation calculation of compression damage. Compression damage mainly occurs near the two supports at the lower part of the specimen. Because it is the reverse stress part of the specimen, a large degree of compression damage occurs.

Figure 12 shows a schematic diagram of tensile and compressive damage of micropile-reinforced concrete attached with steel pipes. The damage degree of the main tensile damage part on the upper part of the specimen is smaller than that of the exposed micropile concrete specimen under the protection of external steel pipes, and the part with damage value of 0.9 (red area in Figure 12) is scattered. In addition, the compression damage also mainly occurs near the concrete bearing, which distribute in a small range, the damage degree is lower, and the distribution is strip-like and local block-like.

Taking a micropile with diameter of 140 mm as the representative, the damage results of concrete on different sections are listed in Table 3 based on the section shown in Figure 13. As shown in Table 3, the micropile concrete attached with steel pipes (140-ggh) has improved their tensile and compressive damages on different sections than that on the exposed micropile concrete (140-lgh). The specimens with a diameter of 140 mm of micropile concrete are listed as representatives. The red area of tensile damage at 0.25 m on the left side of the 140-lgh specimen in Table 3 has covered most of the cross sections, while the red area of tensile damage of the 140-ggh specimen is only dotted under the protection of steel pipes, and the rest of the cross section is a safer blue area. On the section with the most obvious tension (0.5 m) of the two types of specimens, the 140-ggh damage red area (representing the working failure part of the specimen) is only half of the same section of the 140-lgh specimen. The damage laws of different interfaces in Table 3 can be summarized as follows: the tensile damage decreases from both ends to the support, which reaches the maximum at the support, and it is almost unaffected in the middle region of the two supports. The compression damage is the maximum at the support and gradually decreases to both sides.

As shown in Figure 14, the load-displacement curve of reinforced concrete with external steel pipes for the micropile is characterized by plastic deformation. In addition, as the diameter of the micropile increases, the load bearing capacity of the specimen also increases. Figure 15 is the tensile damage-load relationship diagram of the five sections of the externally attached steel tube-reinforced concrete micropile. It can be seen that the tensile damage develops faster, and the larger damage is mainly distributed at the tensile parts at both ends of the specimen. As the loading progresses, the damage value tends to 0.9, so the tensile performance of the concrete at this point has already failed.

The above numerical calculation results all show that the flexural and tensile mechanical properties of the micropile specimens with external steel pipes have been improved to a certain extent, and the damage and failure parts of the specimens have changed from a large area distribution to a scattered distribution. The bending and tensile design and construction of the concrete-filled steel tube micropile of the project can provide a certain reference.

4. Practical Formula for Lateral Bearing Capacity of External Steel Tube-Reinforced Concrete Micropile

4.1. Formula. From the current available data, it can be known that the calculation of the lateral bearing capacity of a concrete-filled steel tube column can be performed as follows [28]:

$$V_0 = A_c f_{cv} + A_{s1} f_{sv1} + A_{s2} f = 0.2 A_c f_c + 0.6 A_{s1} f_{s1} + 0.6 A_{s2} f_{sv2} = 0.2 A_c f_c \left[1 + 3 \frac{A_{s1} f_{s1} + A_{s2} f_{sv2}}{A_c f_c} \right], \tag{6}$$

where V_0 is the bearing capacity of concrete-filled steel tube under shear; A_c is the cross-sectional area of the core concrete in the steel tube; f_c is the compressive strength of the core concrete; f_{cv} is the shear strength of the core concrete; A_{s1} is the cross-sectional area of the outer steel tube; and f_{s1} is the outside. The tensile strength of the steel pipe; f_{sv1} is the shear strength of the outer steel pipe; f_{sv2} is the shear strength of the inner steel pipe; A_{s2} is the cross-sectional area of the inner steel pipe; and f_{s2} is the tensile strength of the inner steel pipe.

Through the parameter analysis, it can be known that the damage value of the micropile concrete in the test in this paper has a certain functional relationship with the load. The author selects the part of the specimens where the damage develops faster and have larger distribution area located at the support for formula fitting. For the test piece in this paper in the elastic stress stage, the following can be obtained by fitting:

$$\mathrm{DA} = 0.968 - 2.337 e^{-0.048F}, \tag{7}$$

where DA is the tensile damage value and F is the loading force of the micropile.

After the micropile is subjected to lateral force, damage cracks will appear before the internal concrete is destroyed, which will weaken the lateral bearing capacity of the micropile to a certain extent. Therefore, the author reduced the lateral bearing capacity of the concrete in the micropile correspondingly according to the load on the specimen. That is, as the load increases, the damage value of the most unfavorable part of the pile is multiplied by the unloaded strength of the concrete, so that the bearing capacity of the micropile can be adjusted accordingly.

Considering the influence of the tensile damage on the bearing capacity of the micropile attached to the steel pipe, equation (6) can be rewritten as

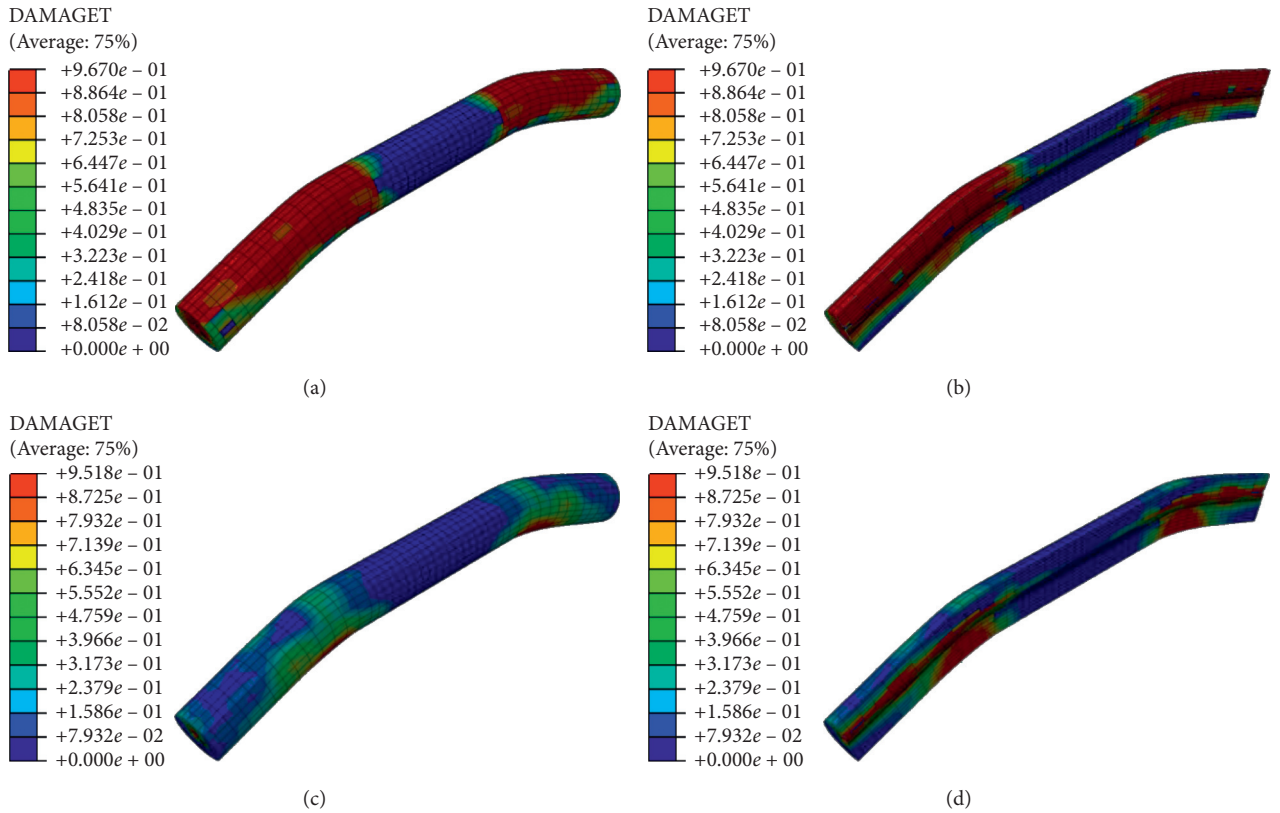

Figure 11: Numerical calculation results of damage of exposed-reinforced concrete miniature piles. (a) Tensile damage (LGH). (b) Tensile damage of 1/2 section (LGH). (c) Compression damage (LGH). (d) Compression damage of 1/2 section (LGH).

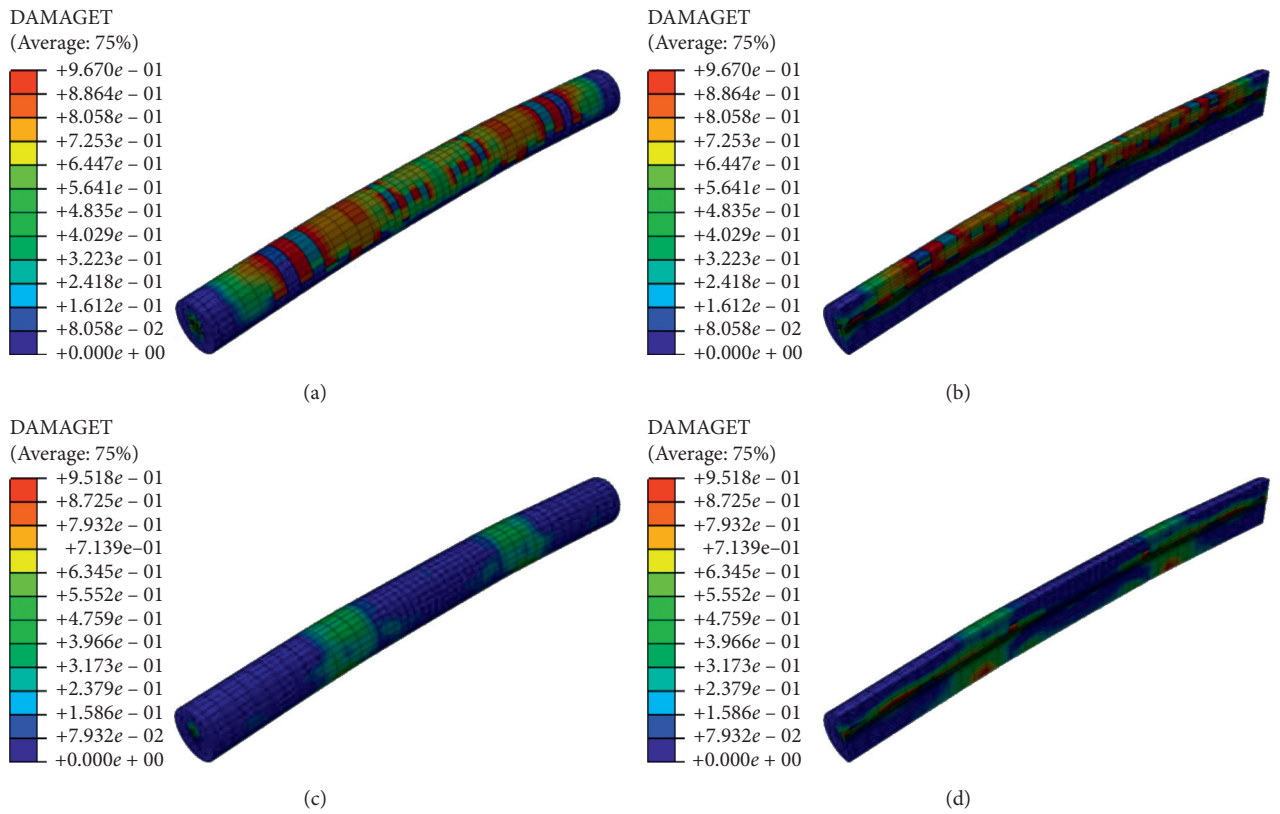

Figure 12: Numerical calculation results of damage of externally attached steel tube-reinforced concrete micropile. (a) Tensile damage (GGH). (b) Tensile damage of 1/2 section (GGH). (c) Compression damage (GGH). (d) Compression damage of 1/2 section (GGH).

Table 3: Calculation results of damage of different sections.

140-LGH		140-GGH	
DAMAGET	DAMAGEC	DAMAGET	DAMAGEC
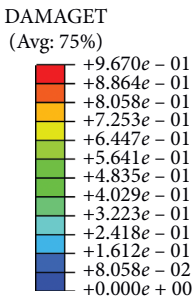	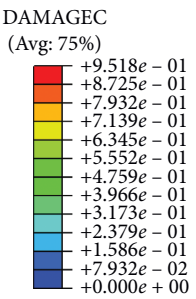	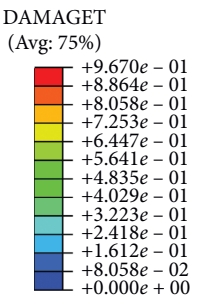	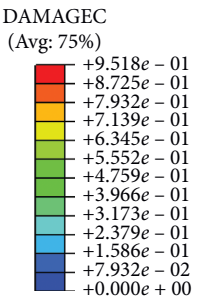
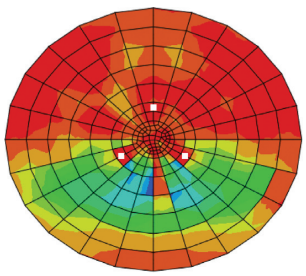	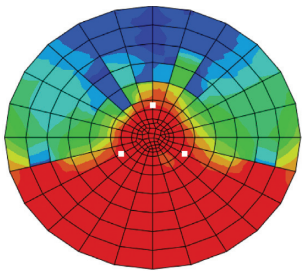	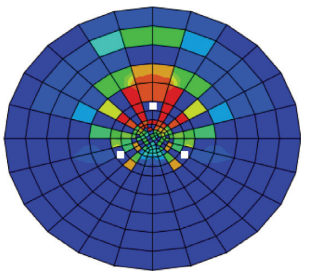	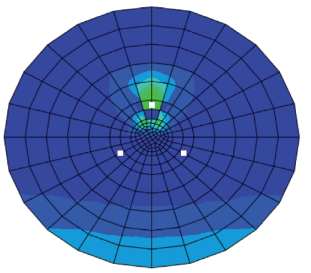
0.25 m	0.35 m	0.25 m	0.25 m
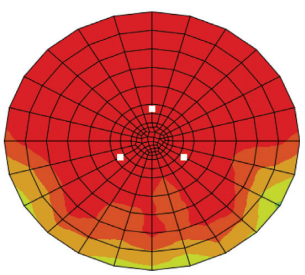	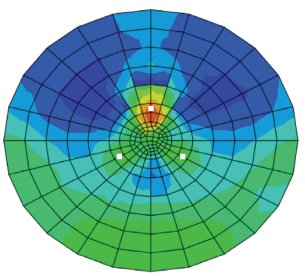	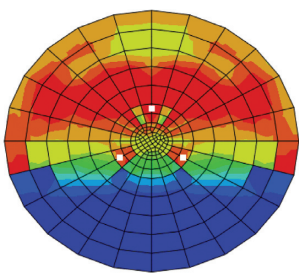	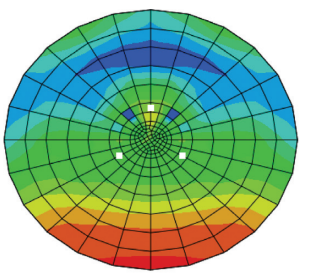
0.5 m	0.5 m	0.5 m	0.42 m
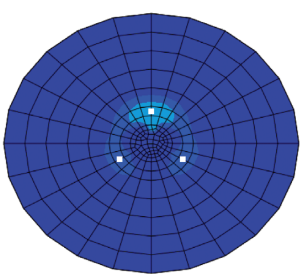	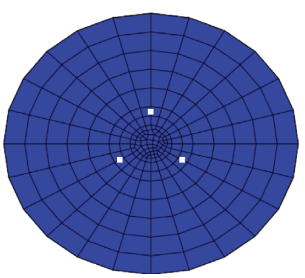	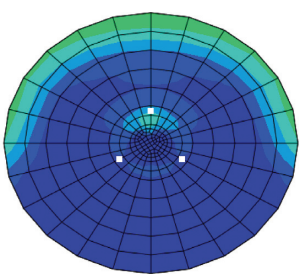	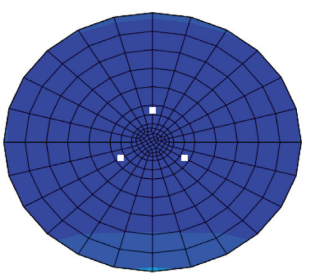
0.75 m	0.75 m	0.75 m	0.75 m
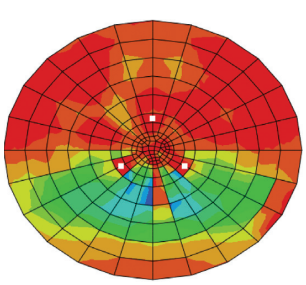	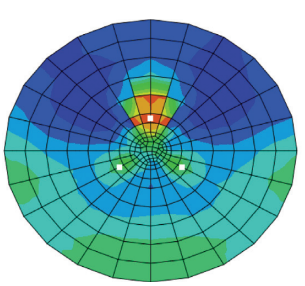	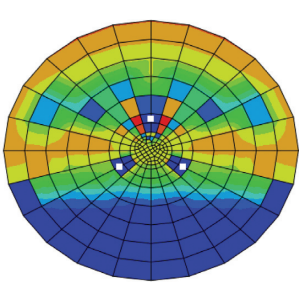	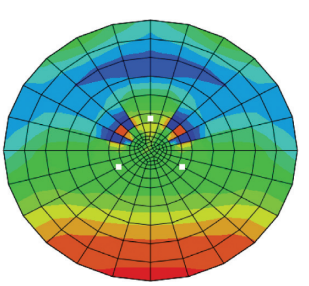
1.0 m	1.0 m	1.0 m	1.08 m

Table 3: Continued.

140-LGH		140-GGH	
DAMAGET	DAMAGEC	DAMAGET	DAMAGEC
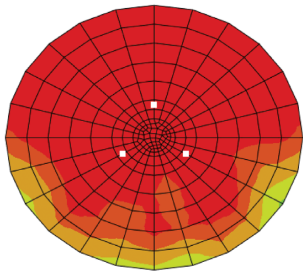	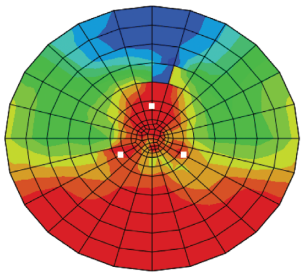	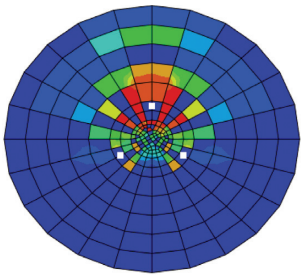	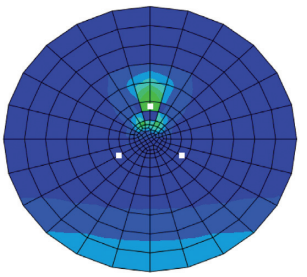
1.25 m	1.20 m	1.25 m	1.25 m

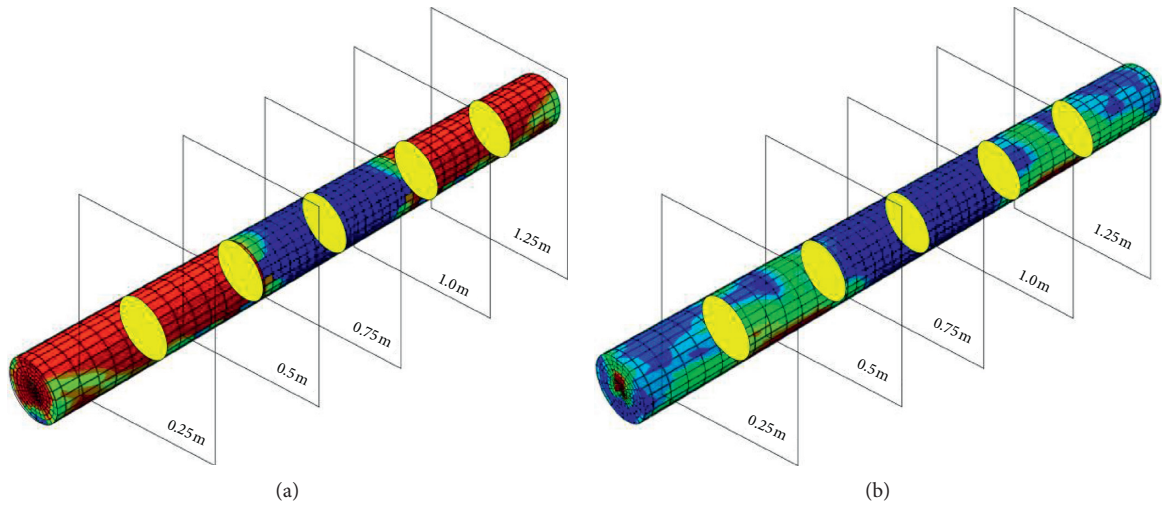

(a) (b)

Figure 13: Concrete damage of different sections. (a) Different sections of tensile damage. (b) Different sections of compression damage.

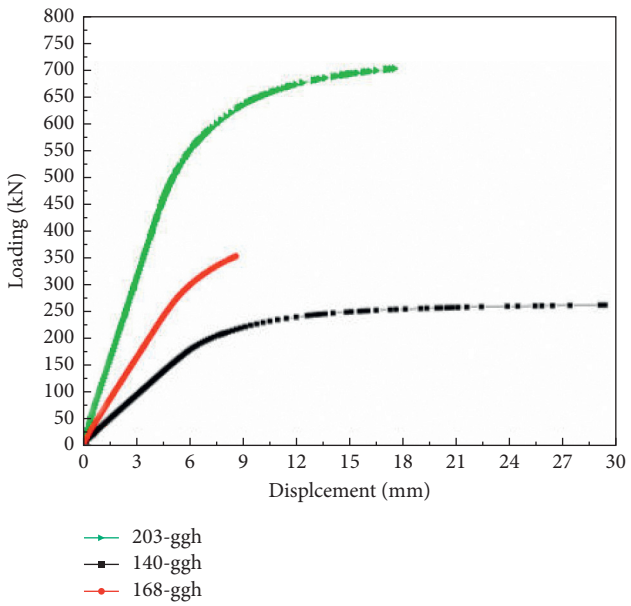

Figure 14: Load-displacement numerical results.

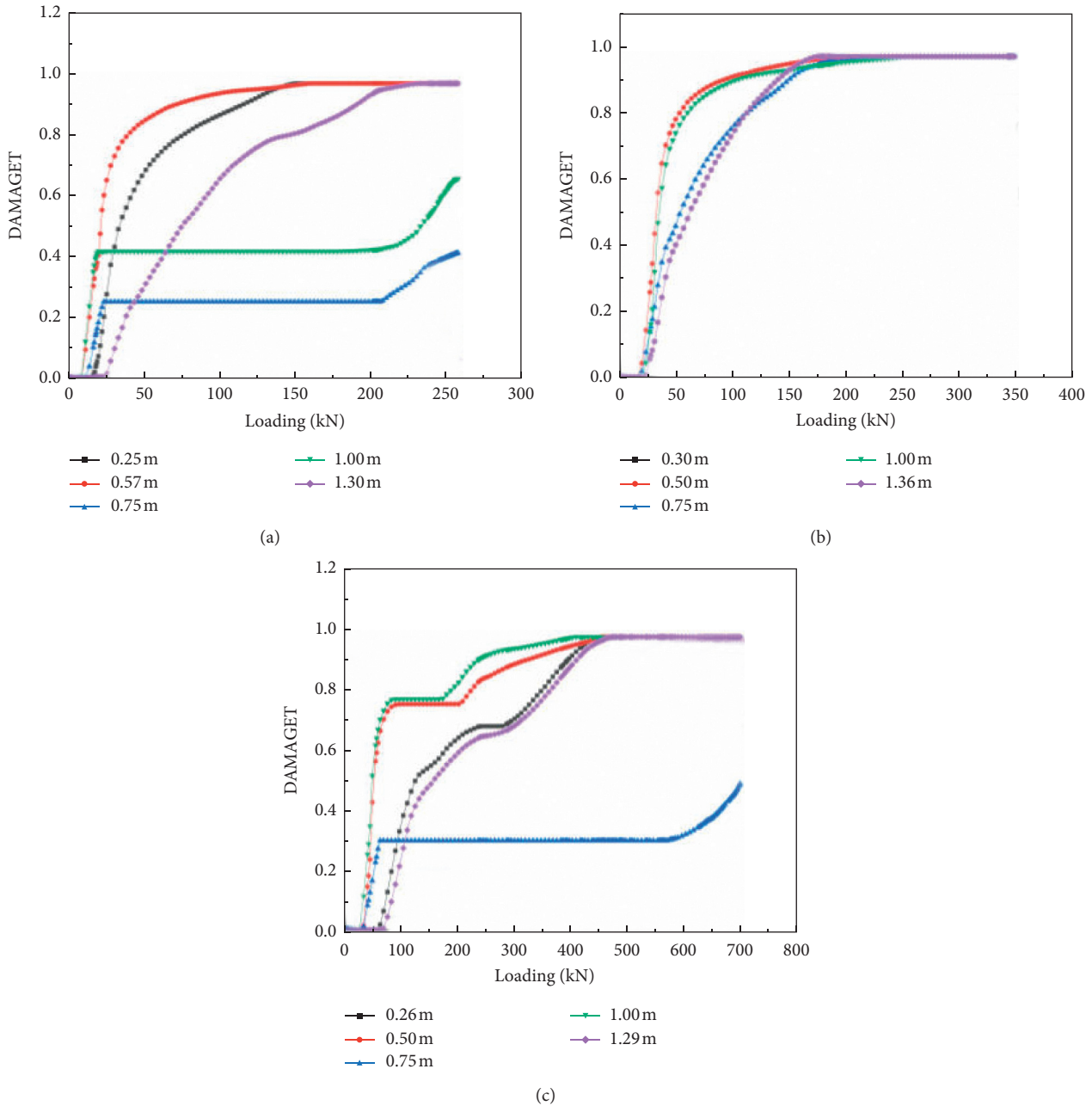

Figure 15: Numerical results of load-tensile damage. (a) 140-ggh. (b) 168-ggh. (c) 203-ggh.

$$V_0 = A_c f_{cv} DA + A_{s1} f_{sv1} + A_{s2} f_{sv2} = 0.2 A_c f_c DA + 0.6 A_{s1} f_{s1} + 0.6 A_{s2} f_{sv2}. \quad (8)$$

The comparison between the 40 sets of finite element calculation results V_{b1} and the calculation result V_{b2} of the transverse bearing capacity equation (8) of the concrete-filled steel tube micropile in this paper is shown in Figure 16. It can be seen from the figure that the two are in good agreement, and the difference is mostly within 10%.

4.2. Comparison of Various Calculation Formulas. Table 4 lists the calculation formulas of different scholars on the lateral bearing capacity of concrete-filled steel tube columns. Table 5 shows the comparison of the test results of the lateral bearing capacity of the concrete micropile with external steel pipes, the finite element calculation results, and the calculation results of equations in Table 4. In Table 5, V_{be} is experimental value, and V_b is the calculation result of finite element and various formulas. It can be seen that the finite element calculation results have the best accuracy and

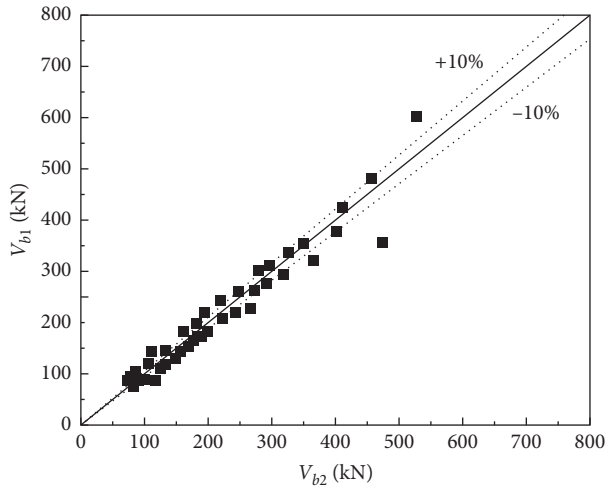

Figure 16: Comparison of $(V)_{b1}/(V)_{b2}$ calculation results.

Table 4: Practical calculation equation for transverse bearing capacity of concrete-filled steel tube columns.

Serial number	Built-in reinforcement	Reference	Equation
1	No	Zhang et al. [29]	$V_u = 1.3V_0(1 - 0.3\sqrt{\lambda})$ $V_0 = 0.2A_c f_c + 0.6A_{s1} f_{s1} + 0.6A_{s2} f_{sv2}$
2	Yes	Zhang et al. [30]	$V_u = k_u V_i$ $V_i = 0.29 f_c'(0.8A_g) + A_{sh} f_{yv} D'\pi/2s + (D-c)N/2a$

Table 5: Comparison of test results and calculation results of transverse bearing capacity of the concrete-filled steel tube micropile.

Built-in reinforcement	Source of the specimens	Total number of specimens	Characteristic value	$V_{b,e}/V_b$		
				FE	Equation (8)	Equations in Table 4
No	Zhang et al. [29]	17	Average	0.982	0.996	1.029
			Coefficient of variation	0.042	0.111	0.050
	This paper	9	Average	0.988	1.013	1.112
			Coefficient of variation	0.051	0.083	0.075
	All above	26	Average	0.993	1.020	1.134
			Coefficient of variation	0.057	0.053	0.197
Yes	Zhang et al. [30]	21	Average	0.970	0.952	1.107
			Coefficient of variation	0.132	0.195	0.204
	This paper	9	Average	1.013	0.993	0.984
			Coefficient of variation	0.074	0.095	0.118
	All above	30	Average	0.982	0.962	0.989
			Coefficient of variation	0.107	0.114	0.154

the smallest dispersion. Equation (8) is equivalent to equations in Table 4 in terms of accuracy and dispersion, but equation (8) proposed in this article is more concise.

Figure 17 shows the comparison between the results of calculation equation (8) proposed by the authors and the test results.

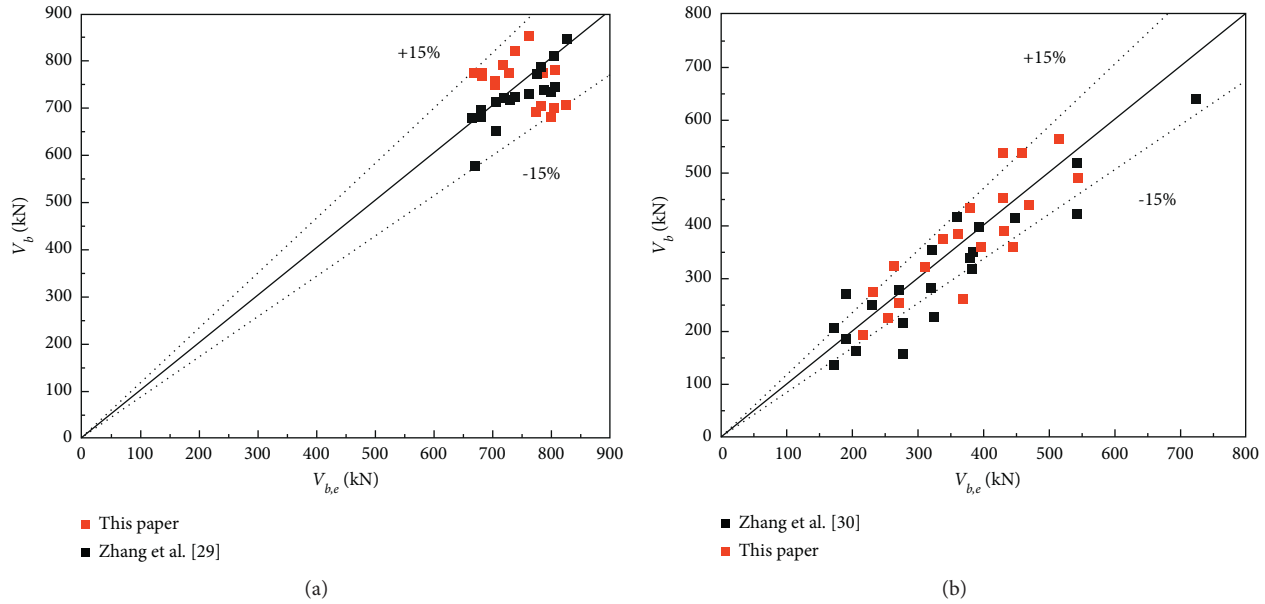

FIGURE 17: Comparison of test results with the calculation equation proposed in this paper. (a) Comparison of the calculation results of the literature [29] and this paper. (b) Comparison of the calculation results of the literature [30] and this paper.

5. Conclusion

(1) The experimental force-displacement mechanical properties of micropile-reinforced concrete show the characteristics of brittle material changes, which are mainly manifested in that after the loading force reaches the elastic limit of the specimen, the load bearing capacity of the specimen decreases sharply, and the test phenomenon on the surface of the specimen is justified. The crack rapidly developed into a gap of 2-3 cm, and the steel and concrete peeled off, and the specimen was damaged.

(2) Compared with the bare-reinforced concrete micropile, the tensile strength curve of the reinforced concrete specimen of the micropile with external steel pipe is the characteristic of plastic material change. After reaching the elastic deformation limit, its deformation will be under the same load force increment. Shows a more obvious change than before.

(3) Under the test loading conditions of bare-reinforced concrete micropile, the tensile damage is mainly distributed in the tension part at both ends of the pile body and expands to the middle part until the bottom support. As the loading force increases to the ultimate elastic strength of the test specimen, the tensile damage value of this part reaches 0.9, so the specimen has already failed. In addition, the compression damage failure part has a small distribution range and is distributed near the bottom support in a block pattern, which is related to the test setup conditions, and the remaining parts have no failure due to compression.

(4) The micropile with external steel pipe is more safe to bear the force. In the test, the load bearing capacity of the specimen before and after is increased by 70%. At the same time, because the tensile damage failure part is distributed in scattered points, the compression damage also mainly appears on the bottom support. Seat, but the distribution range is significantly reduced.

Data Availability

The data used to support the findings of this study are available from the corresponding author upon request.

Conflicts of Interest

The authors declare that they have no conflicts of interest.

Acknowledgments

The authors gratefully acknowledge the support from the projects funded by the Guizhou Province Basic Research Project ([2020]1Y250), Guizhou Province Science and Technology Support Plan Project ([2020]2Y036), Guizhou University Talent Introduction Research Project (GDRGHZ(2017)62), Guizhou Province Ordinary Colleges and Universities Youth Science and Technology Talent Growth Project ([2021]101), and China Postdoctoral Science Foundation (2017M622929).

References

[1] Q. Abbas, W. Choi, G. Kim, I. Kim, and J. Lee, "Characterizing uplift load capacity of micropiles embedded in soil and rock considering inclined installation conditions," *Computers and Geotechnics*, vol. 132, Article ID 103995, 2021.

[2] M. C. Capatti, F. Dezi, S. Carbonari, and F. Gara, "Dynamic performance of a full-scale micropile group: r," *Soil Dynamics and Earthquake Engineering*, vol. 128, Article ID 105858, 2020.

[3] Z. Q. Chen, S. J. Shuai, and S. T Pu, "Experimental study on flexural bearing capacity of micropiles[J]," *Journal of Yangtze River Scientific Research Institute*, vol. 37, no. 2, pp. 100–105, 2020, (in Chinese).

[4] F. Ding, X. Ying, L. Zhou, and Z. Yu, "Unified calculation method and its application in determining the uniaxial mechanical properties of concrete," *Frontiers of Architecture and Civil Engineering in China*, vol. 5, no. 3, pp. 381–393, 2011.

[5] Y. A. Eiaziza, *Performance of Hollow Bar Micropiles under Axial and Lateral Loads in Cohesive soils*, The University of Western Ontario, Ontario, Canada, 2012.

[6] GB50017-2017, *Design of Steel structures*, China Planning Press, Beijing, China, (in Chinese), 2017.

[7] GB/T228-2016, *Metallic Materials-Tensile Testing at Ambient Temperatures*, Standards Press of China, Beijing, China, (in Chinese), 2016.

[8] GB/T50081-2016, *Standard for Method of Mechanical Properties on Ordinary concrete*, China Building Industry Press, Beijing, China, (in Chinese), 2016.

[9] Y. Gunawardena and F. Aslani, "Static flexural behaviour of concrete-filled spiral-welded stainless-steel tubes," *Thin-Walled Structures*, vol. 151, Article ID 106731, 2020.

[10] Z. Guo and L. Deng, "Field behaviour of screw micropiles subjected to axial loading in cohesive soils," *Canadian Geotechnical Journal*, vol. 55, no. 1, pp. 34–44, 2018.

[11] L. Guo, F. Zhou, J. C. Li, Z. Z. Liu, and R. Z. Su, "Numerical simulation analysis and horizontal bearing capacity test of multiple grouting micropiles," *Journal of Nanjing University of Technology (Natural Science Edition)*, vol. 32, no. 6, pp. 64–70, 2010, (in Chinese).

[12] E. D. Haddad and A. J. Choobbasti, "Response of micropiles in different seismic conditions," *Innovative Infrastructure Solutions*, vol. 4, no. 1, 2019.

[13] Y. F. Hu, T. Y. Wang, and L. Ma, "Research on anti-sliding characteristics of single double-row and composite anti-slide micropiles," *Chinese Journal of Rock Mechanics and Engineering*, vol. 31, no. 7, pp. 1499–1505, 2012, (in Chinese).

[14] M. F. Javed, N. H. R. Sulong, S. A. Memon, S. K. U. Rehman, and N. B. Khan, "FE modelling of the flexural behaviour of square and rectangular steel tubes filled with normal and high strength concrete," *Thin-Walled Structures*, vol. 119, pp. 470–481, 2017.

[15] M. Khidri and L. Deng, "Field axial cyclic loading tests of screw micropiles in cohesionless soil," *Soil Dynamics and Earthquake Engineering*, vol. 143, Article ID 106601, 2021.

[16] D. Kyung and J. Lee, "Uplift load-carrying capacity of single and group micropiles installed with inclin-ed conditions," *Journal of Geotechnical and Geoenvironmental Engineering*, vol. 143, 2017.

[17] J. H. Dong and Z. Zhang, "Mechanical properties of the combined retaining structure of frame prestressed anchors and micro steel tube piles in deep foundation pits," *Chinese Journal of Rock Mechanics and Engineering*, vol. 38, no. 3, pp. 619–633, 2019, (in Chinese).

[18] P. Wang, *Analysis of Mechanical Response of Deep Foundation Pit Micropile supporting*, Chang'an University, Xi'an, China, 2018.

[19] Z. Hussain, B. Sharma, and T. Rahman, "Micropile group behaviour subjected to lateral loading," *Innovative Infrastructure Solutions*, vol. 4, no. 1, p. 22, 2019.

[20] C. H. Li, X. L. Zhou, X. M. Wei, and P. Z. He, "Steel pipe pile support in foundation pit with special stratum," *Electronic Journal of Geotechnical Engineering*, vol. 21, no. 15, pp. 5073–5085, 2016.

[21] K. Kershaw and R. Luna, "Scale model investigation of the effect of vertical load on the lateral response of micropiles in sand," *DFI Journal: The Journal of the Deep Foundations Institute*, vol. 12, no. 1, pp. 3–15, 2018.

[22] X. L. Liu and B. Li, "Analysis of supporting mechanism of micro-steel-pipe piles in rock foundation pit," *Rock and Soil Mechanics*, vol. 33, no. 1, pp. 217–222, 2012, (in Chinese).

[23] Y. Q. He, S. J. Yang, H. Luo, and R. Chen, "Bulk excavation," *Dictionary Geotechnical Engineering/Wörterbuch GeoTechnik*, vol. 36, no. 2, p. 174, 2014 (in Chinese).

[24] J. K. Yan, Y. P. Yin, Y. M. Men, and J. Liang, "Model test study of landslide reinforcement with micropile grou-ps," *China Civil Engineering Journal*, vol. 44, no. 4, pp. 120–128, 2011, (in Chinese).

[25] J. K. Yan, Y. P. Yin, and J. Ma, "Large scale model test study in single micropile in landslide reinforcement," *Hydrogeology & Engineering Geology*, vol. 39, no. 4, pp. 55–60, 2012, (in Chinese).

[26] Y. Ye, W. Li, and Z.-X. Guo, "Performance of concrete-filled stainless steel tubes subjected to tension: experimental investigation," *Thin-Walled Structures*, vol. 148, Article ID 106602, 2020.

[27] D. P. Zhou, H. L. Wang, and H. W. Sun, "Micropile composite structure and its design theory," *Chinese Journal of Rock Mechanics and Engineering*, vol. 28, no. 7, pp. 1353–1362, 2009, (in Chinese).

[28] Y. Zheng, C. He, and L. Zheng, "Experimental and numerical investigation of circular double-tube concrete-filled stainless steel tubular columns under cyclic loading," *Thin-Walled Structures*, vol. 132, pp. 151–166, 2018.

[29] J. D. Zhang, F. F. Liu, and T. J. Zhao, "Experimental research on the shear resistance performance of concrete-filled double stainless-steel tubular columns," *Journal of Harbin Engineering University*, vol. 40, no. 7, pp. 118–123, 2019, (in Chinese).

[30] Q. Zhang, P. Bing, Z. Y. Wei, and J. X. Gong, "Shear strength model including the efects off deformation for the circur reinforced concrete columns," *Journal of Chongqing University*, vol. 40, no. 11, pp. 72–82, 2017, (in Chinese).